# The 'functional' dyad of scorpion toxin Pi1 is not itself a prerequisite for toxin binding to the voltage-gated Kv1.2 potassium channels

Stéphanie MOUHAT*†, Amor MOSBAH*†, Violeta VISAN‡, Heike WULFF§, Muriel DELEPIERRE¶, Hervé DARBON‖, Stephan GRISSMER‡, Michel DE WAARD** and Jean-Marc SABATIER*†[1]

*Laboratoire International Associé d'Ingénierie Biomoléculaire, Boulevard Pierre Dramard, 13916 Marseille Cedex 20, France, †Laboratoire de Biochimie, CNRS UMR 6560, Boulevard Pierre Dramard, 13916 Marseille Cedex 20, France, ‡Universität Ulm, Albert Einstein Allee 11, 89081 Ulm, Germany, §Department of Physiology and Biophysics, University of California, Irvine, CA 92697, U.S.A., ¶Laboratoire de RMN, Institut Pasteur, CNRS URA 1129, 28 Rue du Dr. Roux, 75724, Paris, France, ‖AFMB, CNRS UPR 9039, 31 Chemin Joseph Aiguier, 13402 Marseille, France, and **Inserm EMI 9931, 17 Rue des Martyrs, 38054 Grenoble Cedex 09, France

Pi1 is a 35-residue scorpion toxin cross-linked by four disulphide bridges that acts potently on both small-conductance $Ca^{2+}$-activated (SK) and voltage-gated (Kv) $K^+$ channel subtypes. Two approaches were used to investigate the relative contribution of the Pi1 functional dyad (Tyr-33 and Lys-24) to the toxin action: (i) the chemical synthesis of a [$A_{24}$,$A_{33}$]-Pi1 analogue, lacking the functional dyad, and (ii) the production of a Pi1 analogue that is phosphorylated on Tyr-33 (P-Pi1). According to molecular modelling, this phosphorylation is expected to selectively impact the two amino acid residues belonging to the functional dyad without altering the nature and three-dimensional positioning of other residues. P-Pi1 was directly produced by peptide synthesis to rule out any possibility of trace contamination by the unphosphorylated product. Both Pi1 analogues were compared with synthetic Pi1 for bioactivity. *In vivo*, [$A_{24}$,$A_{33}$]-Pi1 and P-Pi1 are lethal by intracerebroventricular injection in mice ($LD_{50}$ values of 100 and 40 $\mu$g/mouse, respectively). *In vitro*, [$A_{24}$,$A_{33}$]-Pi1 and P-Pi1 compete with $^{125}$I-apamin for binding to SK channels of rat brain synaptosomes ($IC_{50}$ values of 30 and 10 nM, respectively) and block rat voltage-gated Kv1.2 channels expressed in *Xenopus laevis* oocytes ($IC_{50}$ values of 22 $\mu$M and 75 nM, respectively), whereas they are inactive on Kv1.1 or Kv1.3 channels at micromolar concentrations. Therefore, although both analogues are less active than Pi1 both *in vivo* and *in vitro*, the integrity of the Pi1 functional dyad does not appear to be a prerequisite for the recognition and binding of the toxin to the Kv1.2 channels, thereby highlighting the crucial role of other toxin residues with regard to Pi1 action on these channels. The computed simulations detailing the docking of Pi1 peptides on to the Kv1.2 channels support an unexpected key role of specific basic amino acid residues, which form a basic ring (Arg-5, Arg-12, Arg-28 and Lys-31 residues), in toxin binding.

Key words: functional dyad, $K^+$ channel, Kv1.2 channel, phosphorylated tyrosine, Pi1, scorpion toxin.

## INTRODUCTION

Pi1 is a scorpion toxin that has been purified from the venom of *Pandinus imperator* (Table 1A) [1–3]. It is a 35-mer peptide cross-linked by four disulphide bridges that are organized according to the conventional pattern of the four-disulphide-bridged scorpion toxins (i.e. C1–C5, C2–C6, C3–C7 and C4–C8) [3,4]. The 3D (three-dimensional) structure of synthetic Pi1 in solution, as determined by $^1$H-NMR [5], shows that the toxin adopts the $\alpha/\beta$ scaffold (i.e. an $\alpha$-helix connected to an anti-parallel $\beta$-sheet by two disulphide bridges) common to most characterized scorpion toxins independent of their size and selectivity towards the various ion channels [6]. Together with MTX (maurotoxin from the scorpion *Scorpio maurus palmatus*) [7,8] and HsTx1 (toxin 1 from the scorpion *Heterometrus spinnifer*) [9], Pi1 belongs to a structural class referred to as $\alpha$-KTx6 [10]. Pi1 has been described previously to act on both rat SK channels (small-conductance $Ca^{2+}$-activated channels) and Kv1.2 channel subtype of the Kv channels (voltage-gated mammalian $K^+$ channels) [1–3]. A number of previous structure–activity relationship studies on different short-chain scorpion toxins strongly suggest that the $\alpha$-helical domain plays a key role in the recognition of SK channels, whereas the $\beta$-sheet structure is more likely to be involved in bioactivity on Kv channels [11–14]. For the latter channels, the functional dyad composed of a basic Lys (entering by its side chain into the ion-channel pore) and an aromatic Tyr (or Phe) is thought to be a crucial structural element regarding the binding properties and blocking activities of these toxins [13,15–17]. Here we have investigated the relative contribution of the Pi1 functional dyad (composed of Lys-24 and Tyr-33) to the toxin action on the voltage-gated Kv1.2 channel, as well as SK channels. Two approaches were used. The first one relied on the synthesis of a [$A_{24}$,$A_{33}$]-Pi1 analogue, a structural analogue of Pi1 lacking the functional dyad, with Ala residues at positions 24 and 33, whereas the second one consisted of the production of P-Pi1, an analogue of Pi1 that is phosphorylated at Tyr-33. A molecular modelling approach has been used to define the phosphorylation of Tyr-33 as an appropriate structural modification of the dyad that should not affect the rest of the molecule in terms of spatial positioning of other residues involved in the putative interacting surface (i.e. the $\beta$-sheet). The Tyr-33-phosphorylated Pi1 product (P-Pi1) was chemically

Abbreviations used: Pi1, toxin 1 from the scorpion *Pandinus imperator*; P-Pi1, Pi1 that is phosphorylated at Tyr-33; [$A_{24}$,$A_{33}$]-Pi1, a structural analogue of Pi1 lacking the functional dyad, with Ala residues at positions 24 and 33; Pi2, toxin 2 from *P. imperator*; MTX, maurotoxin from the scorpion *Scorpio maurus palmatus*; Fmoc, $N^{\alpha}$-fluoren-9-ylmethyloxycarbonyl; TFA, trifluoroacetic acid; MALDI-TOF, matrix-assisted laser-desorption ionization–time of flight; 3D, three-dimensional; Kv channel, voltage-gated mammalian $K^+$ channel; SK channel, small-conductance $Ca^{2+}$-activated $K^+$ channel; PDB, Protein Data Bank.

[1] To whom correspondence should be addressed, at Laboratoire de Biochimie (e-mail sabatier.jm@jean-roche.univ-mrs.fr).

**Table 1 Amino acid sequence alignments of scorpion toxins and $K^+$ channel P-domains**

(a) Scorpion toxins (Cys-based alignments). The Cys residues are shown in bold. (b) P-domains. Variable amino acid residues between Kv channel subtypes are in bold. The N- and C-termini are numbered according to the NCBI Data Bank.

(a)

| Toxin | Subfamily | Amino acid sequence |
|---|---|---|
| MTX | 6.2 | $^{1}$VS**C**TGSKD**C**YAP**C**RKQTG**C**PNAK**C**INKS**C**K**C**YG**C**$^{34}$-$NH_2$ |
| Pi1 | 6.1 | $^{1}$LVK**C**RGTSD**C**GRP**C**QQQTG**C**PNSK**C**INRM**C**K**C**YG**C**$^{35}$-$NH_2$ |
| Pi2 | 7.1 | $^{1}$TIS**C**TNPKQ**C**YPH**C**KKETGYPNAK**C**MNRK**C**K**C**FGR$^{35}$-OH |

(b)

| Ion channel | Amino acid sequence |
|---|---|
| KcsA | $^{50}$ERGAPGAQLITYPRALWWSVETATTVGYGDLYPVTL$^{85}$ |
| Rat Kv1.1 | $^{348}$EA**EEAE**S**H**F**S**SIPDAFWWAVV**S**MTTVGYGDM**Y**P**V**TI$^{383}$ |
| Rat Kv1.2 | $^{350}$EA**DERD**S**Q**F**P**SIPDAFWWAVV**S**MTTVGYGDM**V**P**T**TI$^{385}$ |
| Rat Kv1.3 | $^{370}$EA**DDPS**S**G**F**N**SIPDAFWWAVV**T**MTTVGYGDM**H**P**V**TI$^{405}$ |

produced by solid-phase peptide synthesis using the Fmoc ($N^{\alpha}$-fluoren-9-ylmethyloxycarbonyl)/t-butyl strategy [3,18]. Such a direct chemical synthesis of P-Pi1 appears to be a convenient approach to avoid the possibility of trace contamination by the unphosphorylated Pi1 (native Pi1), which might lead to misinterpretation of the biological data. The pharmacology of [$A_{24}$,$A_{33}$]-Pi1 and P-Pi1 have been compared with that of native Pi1.

## EXPERIMENTAL

### Materials

Fmoc-L-amino acids, Fmoc-amide resin and reagents used for peptide synthesis were obtained from PerkinElmer (Shelton, CT, U.S.A.). Fmoc-L-Tyr(phosphate)-OH was purchased from Bachem AG (Bubendorf, Switzerland). Solvents were analytical-grade products from SDS (Peypin, France).

### Chemical synthesis and characterization of the Pi1 peptides

Pi1, P-Pi1 and [$A_{24}$,$A_{33}$]-Pi1 were produced by independent solid-phase syntheses using an automated peptide synthesizer (model 433A; Applied Biosystems). In the three cases, peptide chains were assembled stepwise on 0.4 mmol of Fmoc-amide resin (1 % cross-linked; 0.66 mmol of amino group/g) using 1 mmol of Fmoc-L-amino acid derivatives [3]. The side-chain-protecting groups used for trifunctional residues were: trityl for Cys, Asn and Gln; t-butyl for Ser, Thr, Tyr (syntheses of Pi1 and [$A_{24}$,$A_{33}$]-Pi1) and Asp; pentamethylchroman for Arg and t-butyloxycarbonyl for Lys. For the synthesis of P-Pi1, Fmoc-L-Tyr(phosphate)-OH was used. $N^{\alpha}$-amino groups were deprotected by treatments with 18 and 20 % (v/v) piperidine/*N*-methylpyrrolidone for 3 and 8 min, respectively. After extensive washings with *N*-methylpyrrolidone, the Fmoc-amino acid derivatives were coupled (20 min) as their hydroxybenzotriazole active esters in *N*-methylpyrrolidone (2.5-fold excess). After complete assembly of the peptides, and removal of their N-terminal Fmoc groups, the peptide resins (≈2.2 g) were treated under stirring for 2.5 h at room temperature with mixtures of TFA (trifluoroacetic acid)/water/thioanisole/ethanedithiol (88:5:5:2, by vol.) in the presence of crystalline phenol (2.25 g) in final volumes of 30 ml/g of peptide resins. The peptide mixtures were then filtered and the filtrates were precipitated and washed twice by adding cold diethyloxide. The crude peptides were pelleted by centrifugation (2800 ***g***, 10 min) and the supernatants were discarded each time. The products were dissolved in water and freeze dried. The reduced peptides were then solubilized (≈1 mM) in 0.2 M Tris/HCl buffer, pH 8.3, to allow oxidative folding (48 h, 22 °C). The target peptides (Pi1, P-Pi1 and [$A_{24}$,$A_{33}$]-Pi1) were purified to homogeneity by reversed-phase HPLC (PerkinElmer; $C_{18}$ Aquapore ODS 20 $\mu$m, 250 mm × 10 mm) by means of a 60 min linear gradient of 0.08 % (v/v) TFA/0–40 % acetonitrile in 0.1 % (v/v) TFA/water at a flow rate of 6 ml/min ($\lambda = 230$ nm). The purity and identity of the three peptides were assessed by: (i) analytical $C_{18}$ reversed-phase HPLC (Merck; $C_{18}$ Lichrospher 5 $\mu$m, 4 mm × 200 mm) using a 60 min linear gradient of 0.08 % (v/v) TFA/0–60 % acetonitrile in 0.1 % (v/v) TFA/water at a flow rate of 1 ml/min; (ii) amino acid content determination after peptide acidolysis [6 M HCl/2 % (w/v) phenol, 20 h, 120 °C, $N_2$ atmosphere]; and (iii) molecular-mass analysis by MALDI-TOF (matrix-assisted laser-desorption ionization–time of flight) MS or electrospray MS.

### Conformational analyses of Pi1, [$A_{24}$,$A_{33}$]-Pi1 and P-Pi1 by one-dimensional NMR

Each peptide, Pi1, [$A_{24}$,$A_{33}$]-Pi1 or P-Pi1, was dissolved ($10^{-3}$ M) in a mixture of water:$^{2}H_2O$ (9:1, v/v). All $^{1}$H-NMR measurements were obtained on a Bruker DRX 500 spectrometer equipped with an HCN probe and self-shielded triple axis gradients were used. The experiments were performed at 300 K.

### Molecular modelling

The molecular modelling of Kv channel subtypes (Figure 1) has been based on the crystal structure of KcsA solved at 2.0 Å (1 Å ≡ 0.1 nm) resolution [PDB (Protein Data Bank) accession number 1K4C] [19]. The amino acid sequences of domains S5-P-S6 of the rat voltage-gated $K^+$ channel $\alpha$-subunits [20] were aligned with the homologous domain of KcsA and showed ≈31 % sequence identities. The sequence identities between the P-domains of Kv-type ion channels and KcsA are between 46 and 51 % (Table 1B). Based on the high degree of identity, models of the S5-P-S6 regions of rat Kv1.1 (NCBI accession number P10499), Kv1.2 (NCBI accession number P15386) and Kv1.3 (NCBI accession number P15384) channels were generated by using Turbo-Frodo software [21]. After Clustal alignments (ClustalW service at the European Bioinformatics Institute, http://www.ebi.ac.uk/clustalw), the mutations were introduced in the amino acid sequence of KcsA, and the structures of the corresponding Kv channels thus obtained were minimized with CNS software [23]. The final molecular models of the S5-P-S6 regions of the rat Kv1.1, Kv1.2 and Kv1.3 channels adopt 3D structures that are similar to that of the KcsA channel (Table 2). To create molecular models of Pi1 [1,2], [$A_{24}$,$A_{33}$]-Pi1 and P-Pi1 (Figure 2A–2C), a multiple sequence alignment was performed using the ClustalW [24] and FASTA [25] algorithms, and the scoring was done using BLOSUM62 matrices [26]. The residue mutations were performed within the amino acid sequence of MTX (PDB accession number 1TXM) [7,8,27], a scorpion toxin that shares the highest known sequence identity with Pi1 (68 %). The sequence similarity between MTX and Pi1 is 88 %. The model of Pi1 was verified to correlate with the low-resolution 3D structure of Pi1 in solution as obtained by nanoprobe spectroscopy [5]. Of note, the former 3D structure of Pi1, as solved by $^{1}$H-NMR, could not be used since no structural data are available from the Protein Data Bank. The final minimized molecular models of Pi1,

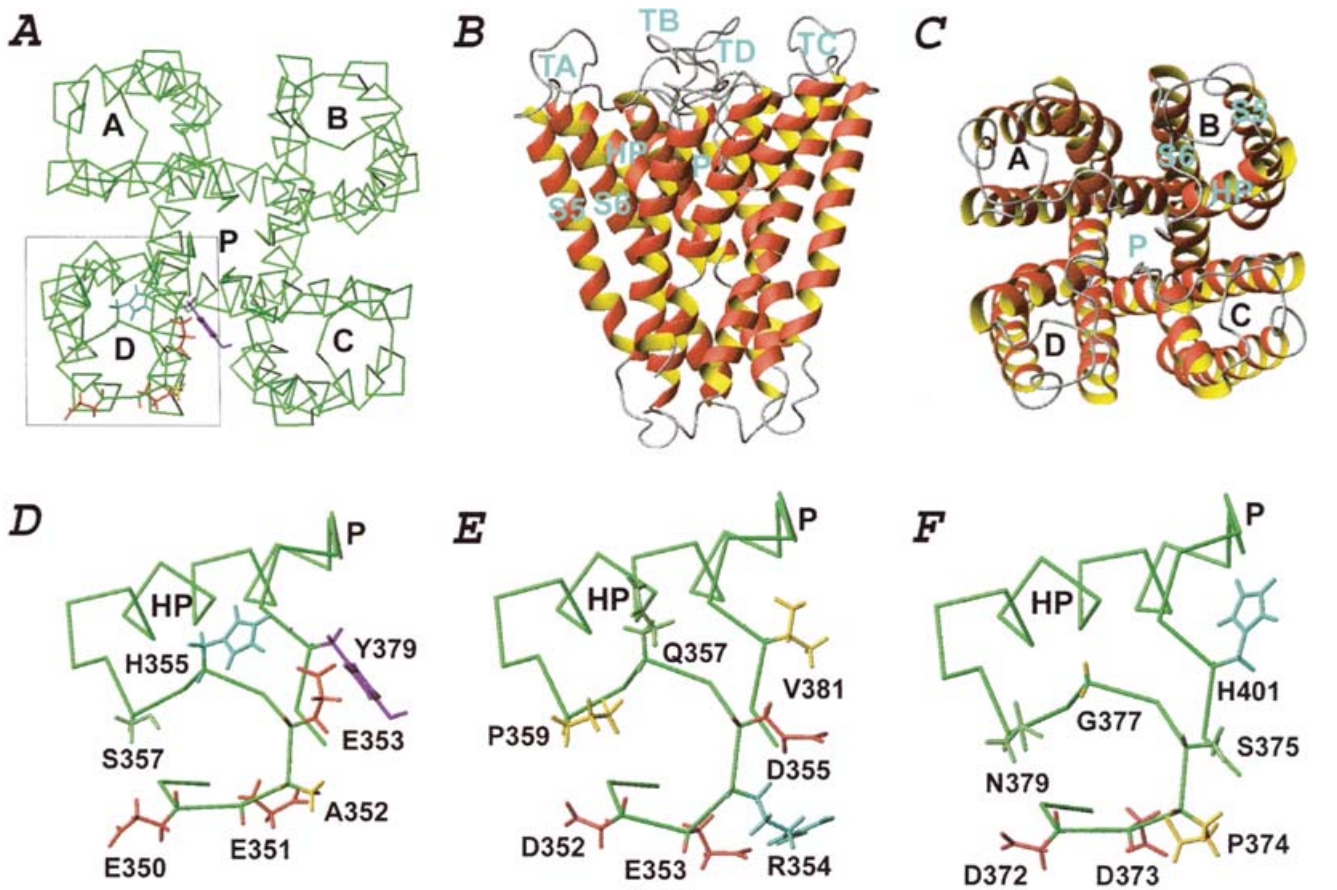


**Figure 1 Molecular models of the rat voltage-gated $K^+$ channels (pore regions)**

(**A**) Top view (Turbo-Frodo software) of the molecular model of a voltage-gated Kv channel (pore regions). The Kv channel is composed of four $\alpha$-subunits [20]. For each $\alpha$-subunit, only the pore region is shown for clarity. It is formed by the transmembrane segment S5, the P-domain (turret region, pore helix and selectivity filter), and the transmembrane segment S6. The four S5-P-S6 $\alpha$-subunits are denoted A– D. The ion channel pore is labelled P. The C$\alpha$ peptide backbone traces are pictured in green. One S5-P-S6 $\alpha$-subunit is boxed (D), detailing the P-domain of the rat Kv1.1 S5-P-S6 $\alpha$-subunit (see panel **D**). (**B**) Side view (Molmol software) of the molecular model of a Kv-type channel (pore regions). The transmembrane helices of segments S5 and S6 are shown in red and yellow. TA–TD indicate turret regions of P-domains (the turret region is located between segment S5 and the $\alpha$-helical structure of P-domain). HP represents the pore helix, i.e. the $\alpha$-helical structure of P-domain (HP is located between the turret region and the selectivity filter). (**C**) Top view of the model shown in (**B**). (**D**–**F**) Molecular models of the P-domains of rat voltage-gated Kv1.1, Kv1.2 and Kv1.3 channel subtypes [20], respectively. P indicates the selectivity filter of the ion-channel pore. Most of the amino acid residues (one-letter code) that differ in the P-domains of the Kv channel $\alpha$-subunits are numbered according to their positions in the $\alpha$-subunit amino acid sequences. The corresponding residue side chains are detailed.

[$A_{24}$,$A_{33}$]-Pi1 and P-Pi1 showed an $\alpha/\beta$ scaffold, with an $\alpha$-helix (from residues 7 to 16), and a two-stranded anti-parallel $\beta$-sheet (residues 23–26 and 29–32).

The quality of all molecular models was assessed using the WHAT IF program [28]. In each case, the stereochemical quality was good and similar to those of the template molecules. The analysis of the molecular models by using the PROCHECK [29] program shows that all models have Ramachandran [30] scores near those of the templates (Table 2). Other stereochemical properties also agree with those of the templates.

### Docking of Pi1, [$A_{24}$,$A_{33}$]-Pi1 or P-Pi1 on to rat Kv1.2 channels

The molecular interaction simulations were performed using the BiGGER docking program [31]. The algorithm used by BiGGER performs a complete and systematic search for surface complementarity (both geometry complementarity and amino acid residue pairwise affinities are considered) between two potentially interacting molecules, and enables an implicit treatment of molecular flexibility. In each case, a population of 1000 candidate protein–protein-docked geometries were selected by BiGGER. In a subsequent step, the putative docked structures were ranked using an interaction scoring function, which combines several interaction terms that are thought to be relevant for the stabilization of protein complexes: geometric packing of the surfaces, electrostatic interactions, desolvation energy and pairwise propensities of the residue side chains to contact across the molecular interface. In the *ab initio* simulations, the entire molecular surface was searched using absolutely no additional information regarding the binding sites. Among the 1000 candidate protein–protein-docked geometries selected, the five best scoring Pi1–Kv1.2, [$A_{24}$,$A_{33}$]-Pi1–Kv1.2 or P-Pi1–Kv1.2 complexes were further treated with the Turbo-Frodo software, taking also into account the proposed functional maps of voltage-gated $K^+$ channel-acting scorpion toxins [16,32–37]. Finally, a rigid body minimization was used to minimize the selected complexes. The best energy solutions, corresponding to the most favourable Pi1–Kv1.2, [$A_{24}$,$A_{33}$]-Pi1–Kv1.2 and P-Pi1–Kv1.2 channel complexes, are presented here (see Figures 6 and 7, below). The *de visu* analysis was done using the Turbo-Frodo software, and the geometric qualities of the structures were verified by PROCHECK 3.3 [38].

**Table 2 Statistics on all molecular models**

Rmsd, root mean square deviation.

| Rmsd | Ion channel . . . | Kv1.3 | Kv1.2 | Kv1.1 | | | | | |
|---|---|---|---|---|---|---|---|---|---|
| Rmsd of all C$\alpha$ versus KcsA (Å) | | 1.56 | 1.54 | 1.49 | | | | | |
| Rmsd of C$\alpha$ of most conserved region versus KcsA (Å) | | 0.67 | 0.68 | 0.68 | | | | | |
| Rmsd of all C$\alpha$ versus Kv1.1 (Å) | | 0.28 | 0.30 | – | | | | | |
| Rmsd of all C$\alpha$ versus Kv1.2 (Å) | | 0.35 | – | 0.30 | | | | | |
| **Rmsd** | **Peptide . . .** | **Pi1** | **P-Pi1** | **[$A_{24}$,$A_{33}$]-Pi1** | | | | | |
| Rmsd of all C$\alpha$ versus MTX (Å) | | 0.99 | 1.12 | 0.99 | | | | | |
| Rmsd of C$\alpha$ of secondary structures versus MTX (Å) | | 0.54 | 0.55 | 0.59 | | | | | |
| Rmsd of all C$\alpha$ versus P-Pi1 (Å) | | 0.26 | – | 0.42 | | | | | |
| Rmsd of all C$\alpha$ versus Pi1 (Å) | | – | 0.26 | 0.15 | | | | | |
| **Ramachandran** | **Ion channel/peptide . . .** | **Kv1.1** | **Kv1.2** | **Kv1.3** | **KcsA** | **Pi1** | **P-Pi1** | **[$A_{24}$,$A_{33}$]-Pi1** | **MTX** |
| Residues in most favoured region | | 258 | 256 | 258 | 245 | 17 | 17 | 20 | 20 |
| | | 75.0% | 74.4% | 75.0% | 74.6% | 58.6% | 60.7% | 68.9% | 68.9% |
| Residues in additional allowed region | | 76 | 76 | 76 | 79 | 10 | 10 | 7 | 9 |
| | | 22.1% | 22.1% | 22.1% | 24.1% | 34.5% | 34.5% | 24.2% | 31.1% |
| Residues in generously allowed region | | 10 | 12 | 10 | 4 | 2 | 1 | 2 | 0 |
| | | 2.9% | 3.4% | 2.9% | 1.2% | 6.9% | 3.5% | 6.9% | 0% |
| Residues in disallowed region | | 0 | 0 | 0 | 0 | 0 | 0 | 0 | 0 |
| Glycine | | 36 | 36 | 36 | 40 | 4 | 4 | 4 | 3 |
| Proline | | 20 | 20 | 20 | 20 | 2 | 2 | 2 | 2 |

### Neurotoxicity of the peptides in mice

Pi1 and its analogues were tested *in vivo* for toxicity by determining the 50% lethal dose ($LD_{50}$) after intracerebroventricular injection into 20 g C57/BL6 mice (approved by the French ethics committee; animal testing agreement number 006573 delivered by the National Department 'Santé et Protection Animales, Ministère de l'Agriculture et de la Pêche'). Groups of four to six mice per dose were injected with 5 $\mu$l of peptide solution containing 0.1% (w/v) BSA and 0.9% (w/v) NaCl.

### Binding of the Pi1 peptides on SK channels from rat brain synaptosomes

Rat brain synaptosomes (P2 fraction) were obtained as described by Gray and Whittaker [39]. Protein content was assayed by a modified Lowry technique. $^{125}$I-Apamin ($\approx$2000 Ci/mmol) was produced as described [39a]. Aliquots of 50 $\mu$l of 0.1 nM $^{125}$I-apamin were added to 400 $\mu$l of synaptosome suspension (0.4 mg of protein/ml). Samples were incubated (1 h at 0 °C) with 50 $\mu$l of one of a series of concentrations of Pi1 or Pi1 analogues ($10^{-4}$–$10^{-14}$ M) in a 500 $\mu$l final volume. The incubation buffer was 25 mM Tris/HCl/10 mM KCl, pH 7.2. The samples were centrifuged and the resulting pellets were washed three times in 1 ml of the same buffer. Bound radioactivity was analysed (Packard Crystal II). The values expressed are the means of triplicate experiments. Non-specific binding, less than 8% of the total binding, was assessed in the presence of an excess (10 nM) of unlabelled apamin.

### Electrophysiology

#### Oocyte preparation

*Xenopus laevis* oocytes (stages V and VI) were prepared for cRNA injection and electrophysiological recordings, as described [40]. Oocytes were prepared by removing the follicular cell layer by enzymic treatment with 2 mg/ml collagenase IA (Sigma) in Barth's medium [88 mM NaCl, 1 mM KCl, 0.82 mM $MgSO_4$, 0.33 mM $Ca(NO_3)_2$, 0.41 mM $CaCl_2$, 2.4 mM $NaHCO_3$ and 15 mM Hepes, pH 7.4, with NaOH]. Linearized plasmids were transcribed by means of a T7 or SP6 mMessage mMachine kit (Ambion). The cRNA were stored frozen in water at $-80$ °C at 1 $\mu$g/$\mu$l. The cells were micro-injected 2 days later with 50 nl of cRNA (0.2 $\mu$g/$\mu$l Kv1.1, Kv1.2 and Kv1.3 channels). To favour Kv channel expression, cells were incubated at 16 °C into a defined nutrient oocyte medium [41] 2–6 days before current recordings.

#### Electrophysiology recordings

Standard two-microelectrode techniques were used at room temperature (19–22 °C) to record oocyte currents. The current and voltage electrodes were filled with 140 mM KCl and had resistances between 0.5 and 1 M$\Omega$. Currents were recorded using a voltage-clamp amplifier (GeneClamp 500; Axon Instruments, Foster City, CA, U.S.A.) interfaced with a 16-bit AD/DA converter (Digidata 1200A; Axon Instruments) for monitoring and voltage protocol application. Current records were sampled at 10 kHz and low-pass-filtered at 2 kHz using an eight-pole Bessel filter and stored on computer for analysis. The extracellular recording solution contained 88 mM NaCl, 10 mM KCl, 2 mM $MgCl_2$, 0.5 mM $CaCl_2$, 0.5 mM niflumic acid and 5 mM Hepes, pH 7.4 (with NaOH). Leak and capacitive currents were subtracted online by a P/4 protocol. Residual capacitive artefacts were blanked for display purposes. The solutions of Pi1, [$A_{24}$,$A_{33}$]-Pi1 or P-Pi1 were superfused in the recording chamber at a flow rate of 2 ml/min using a ValveBank4 apparatus (Automate Scientific). BSA (0.1%, w/v) was added to the recording and perfusion solutions to prevent peptide loss to the plastic chamber, tubules and non-specific binding on to the cells. Data analyses were achieved using pCLAMP 6.0.3 software (Axon Instruments). Kv1.3 currents were also recorded from Jurkat T-cells using the whole-cell patch-clamp technique [42].

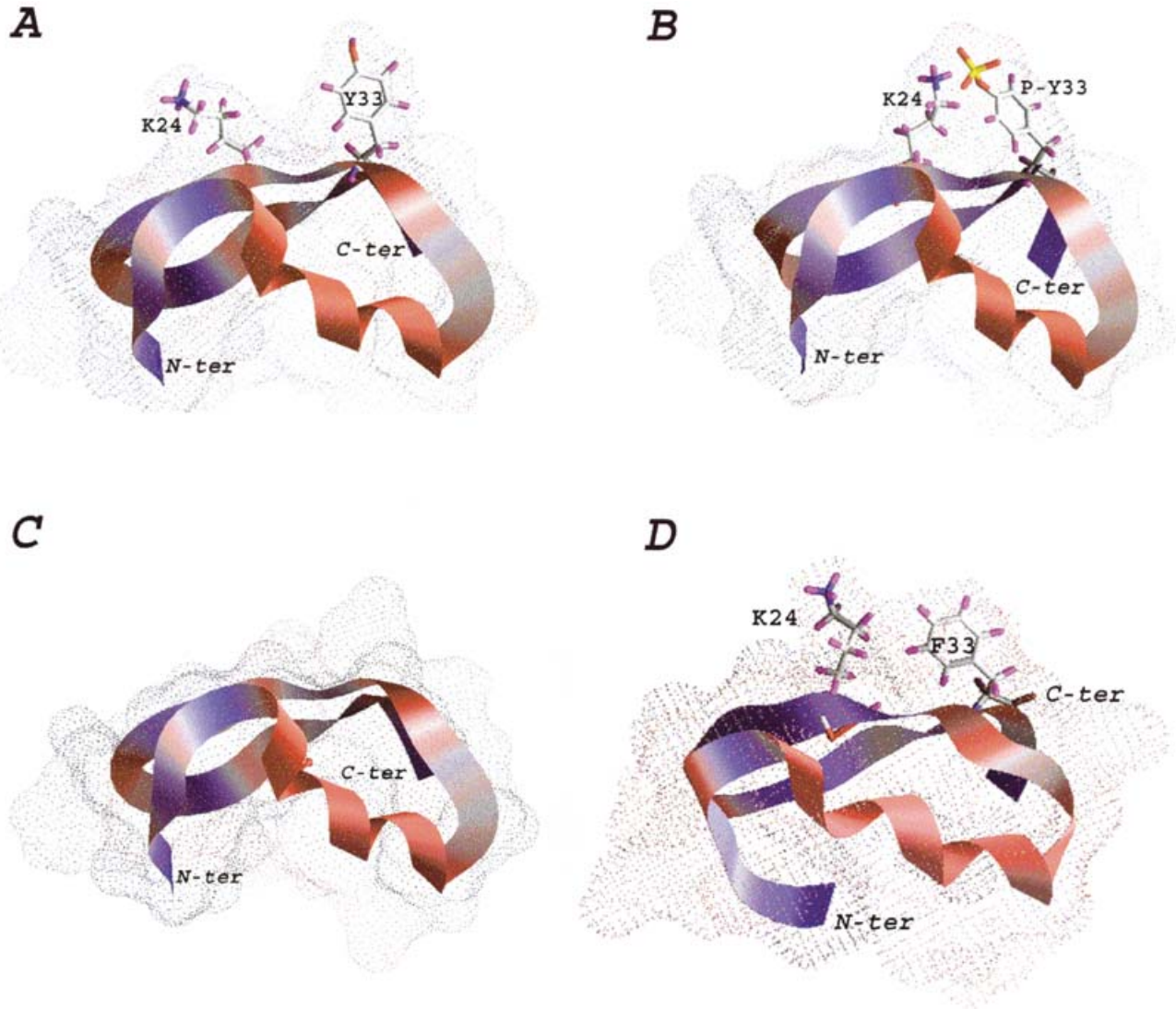


**Figure 2 Molecular models of Pi1, P-Pi1 and [$A_{24}$,$A_{33}$]-Pi1, and 3D structure of Pi2 scorpion toxin**

(**A**–**C**) Molecular models of Pi1 [1–3], its Tyr-33-phosphorylated derivative, P-Pi1, and [$A_{24}$,$A_{33}$]-Pi1, respectively. (**D**) Three-dimensional structure of Pi2 (PDB accession number 2PTA; also referred to as PiTx-K$\alpha$) [46] in solution, as solved by $^1$H-NMR. The ribbon representation (GRASP software) is used to show C$\alpha$ peptide backbones. The side chains of residues belonging to the toxin functional dyads are numbered and detailed in each case. Of note, an aromatic Phe-33 replaces the usual Tyr residue in the case of the Pi2 functional dyad [2,45,46]. The molecular volumes are shown in grey. P-Y33 indicates the phosphorylated Tyr-33 of P-Pi1.

## RESULTS AND DISCUSSION

### Rationale

The aim of this work was to address the role of a pair of topologically well-defined basic Lys and aromatic Tyr (or Phe) residues, referred to as the functional dyad, which is present in the $\beta$-sheet structures of almost all known Kv channel-acting scorpion toxins. Such a dyad is reportedly crucial to the interaction and blockage of voltage-gated $K^+$ channels by scorpion toxins [13,15–17]. An evaluation of the importance of the functional dyad in terms of binding and blockage of the various voltage-gated $K^+$ channels by scorpion toxins should help us to understand better the molecular criteria of channel recognition by the toxin. Basically, the main concern is whether or not the functional dyad is the main determinant for toxin recognition and binding to the voltage-gated $K^+$ channels. Interestingly, the importance of the functional dyad has recently been challenged by the discovery of Tc32, a toxin from the venom of the Amazonian scorpion *Tityus cambridgei*, which blocks (in the low nanomolar concentration range) the voltage-gated Kv1.3 channels but lacks the dyad [43].

In our study, we used Pi1 [1–3] since (i) it possesses a typical $\beta$-sheet-associated dyad formed by Lys-24 and Tyr-33 (Figure 2A), (ii) it potently blocks Kv1.2 channels, with an $IC_{50}$ value in the nanomolar range, and (iii) its 3D structure in solution has been studied by $^1$H-NMR [5].

### Structural modifications of Pi1 that selectively target its functional dyad

To alter selectively the structure of the Pi1 dyad, two different approaches were used. First, we chemically produced a Pi1 analogue in which the dyad was lacking ([$A_{24}$,$A_{33}$]-Pi1; see the molecular model in Figure 2C). Second, we synthesized a Tyr-33-phosphorylated analogue of Pi1 (P-Pi1). The main reasons

for synthesizing the latter were (i) the structural modification of the phenol side chain prevents the occurrence of any hydrogen bonding with other amino acid residues, (ii) one out of the two negatively charged oxygen atoms of the phosphate moiety of the phosphorylated Tyr-33 is expected to form a salt bridge with the positively charged $\varepsilon$-amino group of the Lys-24 side chain that is located in close spatial vicinity, thereby also modifying the properties of Lys-24 from the functional dyad, and (iii) the possible stabilization of the putative interaction between the phosphorylated Tyr-33 and Lys-24 by additional hydrogen bonding between another oxygen atom of the phosphate moiety and the $\varepsilon$-amino group of the Lys-24. According to the molecular model, a salt bridge cannot be formed with the proximal Lys-31 side chain because of a naturally unfavourable orientation of the Tyr-33 phenolic ring, together with distance constraints between phosphorylated Tyr-33 and Lys-31. The theoretical occurrence of a salt bridge between the two residues of the dyad relies on the computer-generated structural model of P-Pi1 (Figure 2B) that has been constructed by using molecular dynamics calculation and energy minimization. It is noteworthy that, although the connection between the phosphorylated Tyr-33 and the side chain of Lys-24 remains speculative, albeit energetically favoured, at least one residue belonging to the dyad of Pi1 has been formerly altered, i.e. Tyr-33.

### Chemical synthesis and characterization of the Pi1 peptides

Pi1, P-Pi1 and [$A_{24}$,$A_{33}$]-Pi1 were produced by three independent stepwise solid-phase syntheses [18] using a standard Fmoc/t-butyl strategy, as described in [3]. Similar yields of peptide chain assembly were obtained for the peptides, ranging from 75 to 85 %. After final deprotection with TFA, the crude reduced peptides were oxidatively folded in 0.2 M Tris/HCl buffer, pH 8.3 (48 h, 22 °C), and purified to complete homogeneity by $C_{18}$ reversed-phase HPLC. The amino acid ratios calculated after acidolysis of the folded products (Pi1, P-Pi1 and [$A_{24}$,$A_{33}$]-Pi1) were in close agreement with the deduced values (results not shown). The MS analyses of Pi1 and [$A_{24}$,$A_{33}$]-Pi1 by the MALDI-TOF technique gave, respectively, experimental molecular masses $(M+H)^+$ of 3834.4 and 3686.8, which are close to the deduced molecular masses $(M+H)^+$ of 3834.5 and 3686.4. For P-Pi1, the experimental molecular mass (electrospray MS) was similar to its deduced molecular mass of 3913.2. Isoelectrofocusing experiments gave a $pH_i$ value of 8.5 for P-Pi1, as compared with 8.9 for Pi1, which also demonstrates the presence of the phosphate moiety in P-Pi1. The final yields of Pi1, P-Pi1 and [$A_{24}$,$A_{33}$]-Pi1 chemical syntheses (which combined peptide chain assembly, final deprotection, folding/oxidation and HPLC purification) were $\approx$2–3 %, which represents average yields similar to those previously obtained for other chemically synthesized scorpion toxins and their structural analogues [3,7,11,12]. It is noteworthy that P-Pi1 was directly produced by using an Fmoc-Tyr(phosphate)-OH derivative (instead of a possible *in vitro* kinase-based phosphorylation of Pi1) in order to prevent any potential trace contamination by unmodified Pi1 during testing of the P-Pi1 sample. As expected, the conformational analyses of Pi1, [$A_{24}$,$A_{33}$]-Pi1 and P-Pi1 by one-dimensional $^1$H-NMR (Figure 3) showed that they all adopt similar 3D structures (similar overall distribution of the resonance frequencies indicating related conformations) that are consistent with folding according to the scorpion toxin $\alpha/\beta$ scaffold (evidence for $\alpha$-helical and $\beta$-sheet structures) [5,6]. Of note, the $^1$H-NMR spectrum of [$A_{24}$,$A_{33}$]-Pi1 is quite different from the spectra of Pi1 and P-Pi1. Most of these differences can be reasonably attributed to the replacement of the Tyr-33 residue of Pi1 or P-Pi1 by an alanyl in [$A_{24}$,$A_{33}$]-Pi1, which alters the strong ring current effect induced by the presence of the Tyr-33 phenol and markedly modifies resonance frequencies of the protons near the ring. Interestingly, we did not notice any significant impact of the phosphorylated Tyr-33 on P-Pi1 oxidative folding, as compared with the Pi1 folding/oxidation *in vitro*, as assessed by $C_{18}$ reversed-phase HPLC at different times of the oxidative folding process (results not shown). For each peptide, the final half-cystine pairings (as assessed by enzyme-based cleavages of the synthetic peptides) were found to be of the conventional types, i.e. C1–C5, C2–C6, C3–C7 and C4–C8 [3].

### Bioactivities of Pi1, [$A_{24}$,$A_{33}$]-Pi1 and P-Pi1

#### Neurotoxicity

The three peptides were compared for their lethal activities by intracerebroventricular injection in mice. The $LD_{50}$ values were 0.2 $\mu$g (Pi1), 100 $\mu$g ([$A_{24}$,$A_{33}$]-Pi1) and 40 $\mu$g (P-Pi1) per mouse, indicating that [$A_{24}$,$A_{33}$]-Pi1 and P-Pi1 are about 500- and 200-fold less potent than Pi1 in an *in vivo* toxicity assay, respectively. In each case, the neurotoxic symptoms observed following these peptide inoculations resemble those obtained when other $K^+$ channel-acting toxins are injected in mice, suggesting that $K^+$ channels are indeed the molecular targets of Pi1 peptides.

#### SK channels

We tested the ability of the peptides to compete with $^{125}$I-labelled apamin for binding to apamin-sensitive SK channels of rat brain synaptosomes [3]. Pi1, [$A_{24}$,$A_{33}$]-Pi1 and P-Pi1 compete with radiolabelled apamin for binding, with respective $IC_{50}$ values of $50 \pm 15$ pM ($n=3$), $30 \pm 6$ nM ($n=3$) and $10 \pm 4$ nM ($n=3$). Therefore, [$A_{24}$,$A_{33}$]-Pi1 and P-Pi1 are 600- and 200-fold less potent than Pi1 in this competition assay, respectively. Although SK channel recognition was previously reported to involve the $\alpha$-helical domain of scorpion toxins [11–14], one cannot rule out that Tyr-33 and/or Lys-24 of Pi1 might also be involved in the interaction of the toxin with SK channels.

#### Kv channels

The efficacy of Pi1, [$A_{24}$,$A_{33}$]-Pi1 or P-Pi1 to block $K^+$ currents from voltage-gated Kv1.1, Kv1.2 or Kv1.3 channels was examined by electrophysiology. We found that Pi1, [$A_{24}$,$A_{33}$]-Pi1 and P-Pi1 are able to block rat Kv1.2 currents with $IC_{50}$ values of $1.3 \pm 0.1$ nM ($n=5$), $22 \pm 4$ $\mu$M ($n=3$) and $75 \pm 7$ nM ($n=4$), respectively (approx. 17000- and 58-fold decreases in blocking potency for [$A_{24}$,$A_{33}$]-Pi1 and P-Pi1, respectively; Figure 4). The peptides were without any significant effects on mouse Kv1.1 and Kv1.3 channel subtypes (identical to rat amino acid sequence for the S5-P-S6 region) at micromolar concentrations (results not shown). Although [$A_{24}$,$A_{33}$]-Pi1 and P-Pi1 are much less active than Pi1 both *in vivo* and *in vitro*, the data show that the full integrity of the Pi1 functional dyad is important but not a prerequisite to a toxin action on voltage-gated Kv1.2 channels. Next, we tested whether these Pi1 analogues interacted with Kv1.2 and blocked $K^+$ outflow through the same binding site. In order to evaluate this point, we checked the Kv1.2 channel-blocking efficacies of Pi1 after application of any one of the two analogues (Figure 5). If no competition occurs, the efficacy of Pi1 should be independent of the presence of [$A_{24}$,$A_{33}$]-Pi1 or P-Pi1, whereas a competition for the same binding site should reduce the efficacy of Pi1 block. In our competition experiments, we used 2.5 nM Pi1, which reduces the steady-state peak current by 57 % if no competition occurs (Figure 5A). In Figure 5(B), 20 $\mu$M [$A_{24}$,$A_{33}$]-Pi1 was applied extracellularly in the whole-cell

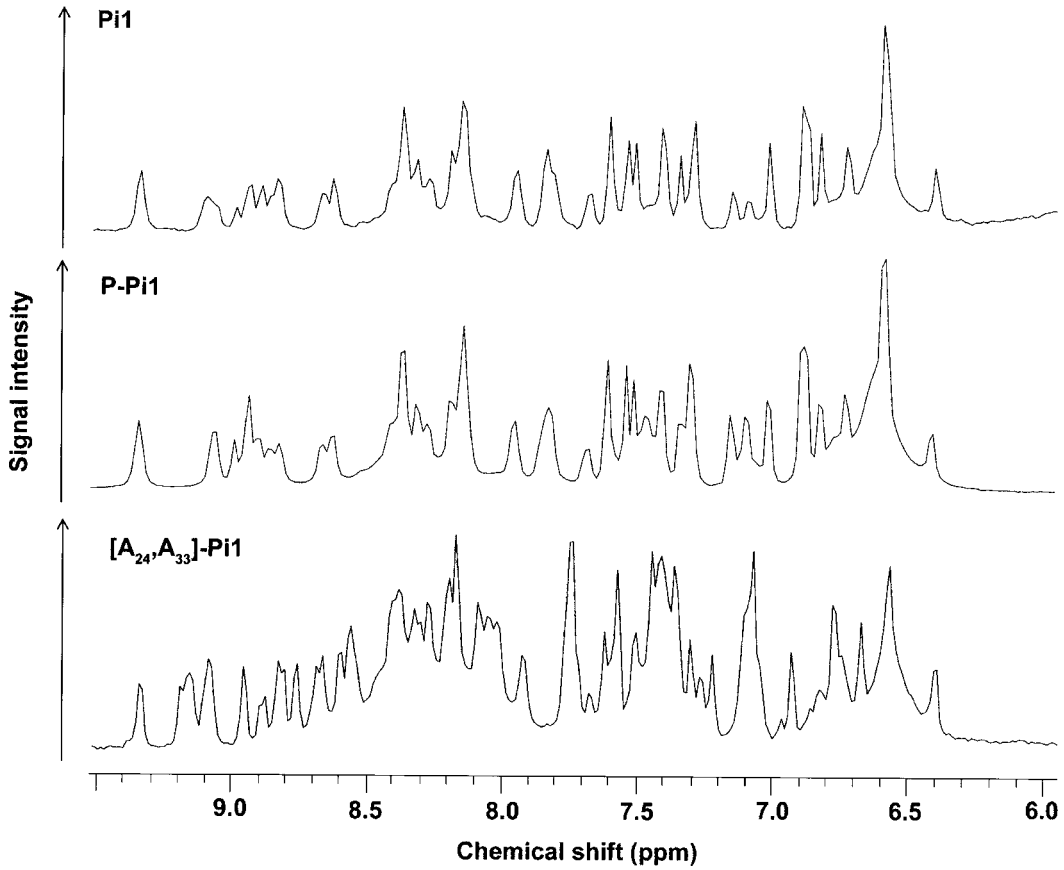


**Figure 3 Structural comparison between Pi1, P-Pi1 and [$A_{24}$,$A_{33}$]-Pi1 using one-dimensional $^1$H-NMR**

One-dimensional $^1$H-NMR spectra of Pi1 (top), P-Pi1 (middle) and [$A_{24}$,$A_{33}$]-Pi1 (bottom). Only the representative amide proton regions are shown. Note that although the spectrum of [$A_{24}$,$A_{33}$]-Pi1 is quite different from the spectra of Pi1 and P-Pi1 (we mostly attributed this difference to the strong ring current effect induced by the Tyr-33 phenol ring in Pi1 or P-Pi1), analysis of the overall distribution of resonance frequencies suggests that the 3D structures of all three peptides are similar.

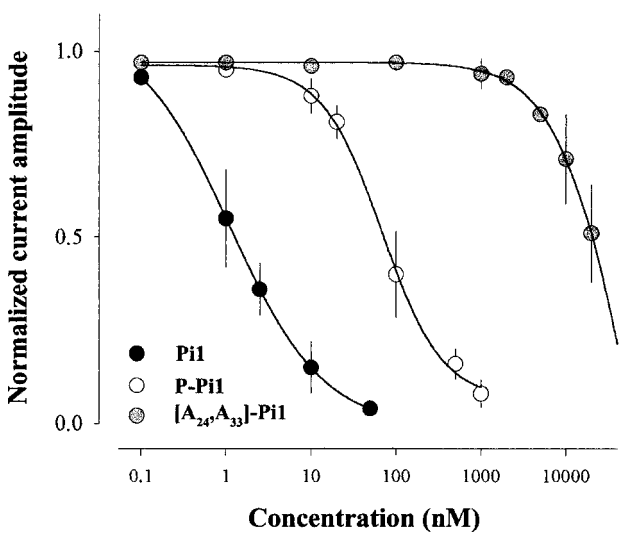


**Figure 4 Affinity of Pi1 and Pi1 analogues for rat Kv1.2 channels**

Dose–response curves of Pi1 peptides to block current through rat Kv1.2 channels. $K^+$ currents were elicited by a train of 10 depolarizing voltage steps to $+60$ mV once every second from a holding potential of $-80$ mV. Each data point corresponds to the mean $\pm$ S.D. from three to seven experiments. Data were fitted to a modified Hill equation, $I_{toxin}/I_{control} = 1/[1 + ([toxin]/K_d)^n]$, with a Hill coefficient $n = 1$.

configuration to the Kv1.2 channel and the $K^+$ current was reduced by 64 % (Figure 5B, middle trace). This reduction of $K^+$ current is specific, since the application of 20 $\mu$M apamin (a highly potent SK channel-acting bee venom toxin), under identical experimental conditions, was without effect on this current (results not shown). The addition of 2.5 nM Pi1 to the 20 $\mu$M [$A_{24}$,$A_{33}$]-Pi1 containing solution led to an additional steady-state current reduction of 20 % of the current level after [$A_{24}$,$A_{33}$]-Pi1 application. This steady-state current reduction is much weaker than the 57 % reduction observed in the absence of [$A_{24}$,$A_{33}$]-Pi1 and suggests that the interaction of Pi1 with the Kv1.2 channel is not independent of the simultaneously applied [$A_{24}$,$A_{33}$]-Pi1. Similar results were obtained when 50 nM P-Pi1 was used instead of 20 $\mu$M [$A_{24}$,$A_{33}$]-Pi1 (Figures 5C and 5D). These results strongly suggest that both peptides are competing for the same binding site as Pi1 on Kv1.2 channel.

Therefore, it seems likely that amino acid residues other than those belonging to the Pi1 dyad play a key role in the recognition and interaction of the toxin with the Kv1.2 channel subtype. In agreement with these data, individual mutations of either the Lys-23 or Tyr-32 residue (functional dyad) of the Pi1 structurally-related MTX to Ala decreased the activity of the peptides towards Kv1.2 channels, with $IC_{50}$ values of 170 nM ([$A_{23}$]-MTX) and 190 nM ([$A_{32}$]-MTX) [44], but did not render them completely inactive. This indicates that, similar to Pi1, the full integrity of the MTX dyad is not a prerequisite to its action on Kv1.2 channel.

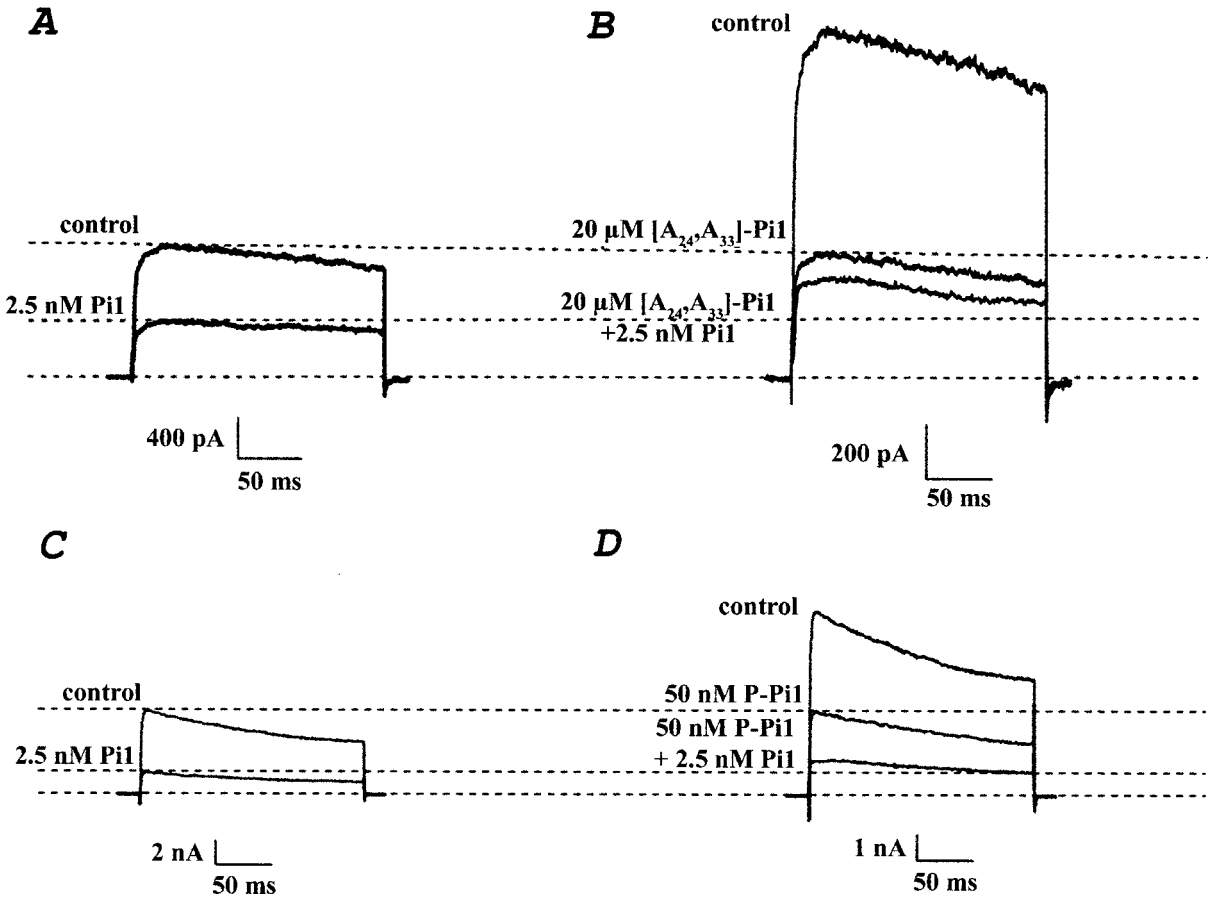


**Figure 5 Effects of Pi1 after [$A_{24}$,$A_{33}$]-Pi1 or P-Pi1 block of Kv1.2 $K^+$ currents**

Currents were elicited by a train of 10 depolarizing voltage steps from a holding potential of −80 to +60 mV once every second. (**A**) Effect of 2.5 nM externally applied Pi1 alone. (**B**) Effect of 20 $\mu$M externally applied [$A_{24}$,$A_{33}$]-Pi1 alone (middle trace) and in combination with 2.5 nM Pi1 (bottom trace). All experiments were done in the whole-cell configuration, using a stable transfected mammalian cell line expressing the rat voltage-gated Kv1.2 channels [42]. Of note, irrelevant peptides (e.g. bee venom toxin apamin, fragment 1–20 of *Shaker* B channel) had no effect on $K^+$ currents when tested up to 20 $\mu$M. (**C**) As in (**A**). (**D**) Effect of 50 nM P-Pi1 applied alone (middle trace) and in combination with 2.5 nM Pi1 (bottom trace). The competition experiments in (**B**) and (**D**) were repeated three times.

The involvement of other residues may provide a reasonable explanation for the fact that Tc32 blocks Kv1.3 channels despite its lack of such a dyad within an $\alpha/\beta$ scaffold [43]. In conclusion, our data strengthen the idea of a multipoint interaction between scorpion toxins and their target ion channels [13,15], and indicate that the 'functional' dyad is more likely involved in $K^+$ current blockage efficacy rather than in the recognition and binding of the toxin to the voltage-gated Kv1.2 channels.

### Dockings of Pi1, P-Pi1 and [$A_{24}$,$A_{33}$]-Pi on to rat Kv1.2 channels

To examine the interaction between the toxin and the channel at the molecular level, we generated models of Pi1, P-Pi1 and [$A_{24}$,$A_{33}$]-Pi1 docked on to the Kv1.2 channel [31].

#### Pi1–Kv1.2 complex

According to the docking model (Figures 6A–6C), the toxin to ion channel complex is stabilized by four salt bridges between the side chains of Asp-355 of each Kv1.2 $\alpha$-subunit (Kv1.2 channel is composed of four $\alpha$-subunits) and Arg-5, Arg-12, Arg-28 and Lys-31 of Pi1. The Lys-24 side chain of Pi1 enters into the Kv1.2 channel pore and is surrounded by the four Asp-379 carbonyl oxygen atoms of the P-domain selectivity filter. The Tyr-33 of Pi1 is part of a highly hydrophobic cluster of aromatic residues consisting of Phe-358, Trp-366, Trp-367 and Tyr-377 from one of the four Kv1.2 $\alpha$-subunits. The phenol ring of Tyr-33 additionally forms a hydrogen bonding with the $N^{\varepsilon}$ of the Trp-366 indole ring. Some hydrophobic interactions are also likely to occur between aliphatic Ile-26 of Pi1 and Val-381 of the rat Kv1.2 $\alpha$-subunit (results not shown).

#### P-Pi1–Kv1.2 complex

The interaction between P-Pi1 and the Kv1.2 channel (Figure 6D) is found to be mostly similar to that of Pi1 (Figures 6A–C and 6E), except for Tyr-33 which, when phosphorylated on its phenolic ring, does not point to the aromatic cluster (due to steric hindrance and decreased hydrophobicity upon phosphorylation) and is constrained to reorientate markedly to interact, via the phosphate moiety, with the Lys-24 side chain for its stabilization (Figure 2B). Of note, an interaction between the side chains of Lys-24 and Tyr-33 cannot occur in natural Pi1 due to distance constraints. This new pattern of interaction forces should be associated with the decreased blocking efficacy of P-Pi1 towards Kv1.2 channels. According to the docking simulation of Pi1 or P-Pi1 on to the Kv1.2 channel (Figure 6), one can suggest that Arg-5, Arg-12, Arg-28 and Lys-31 (not being part of the functional dyad),

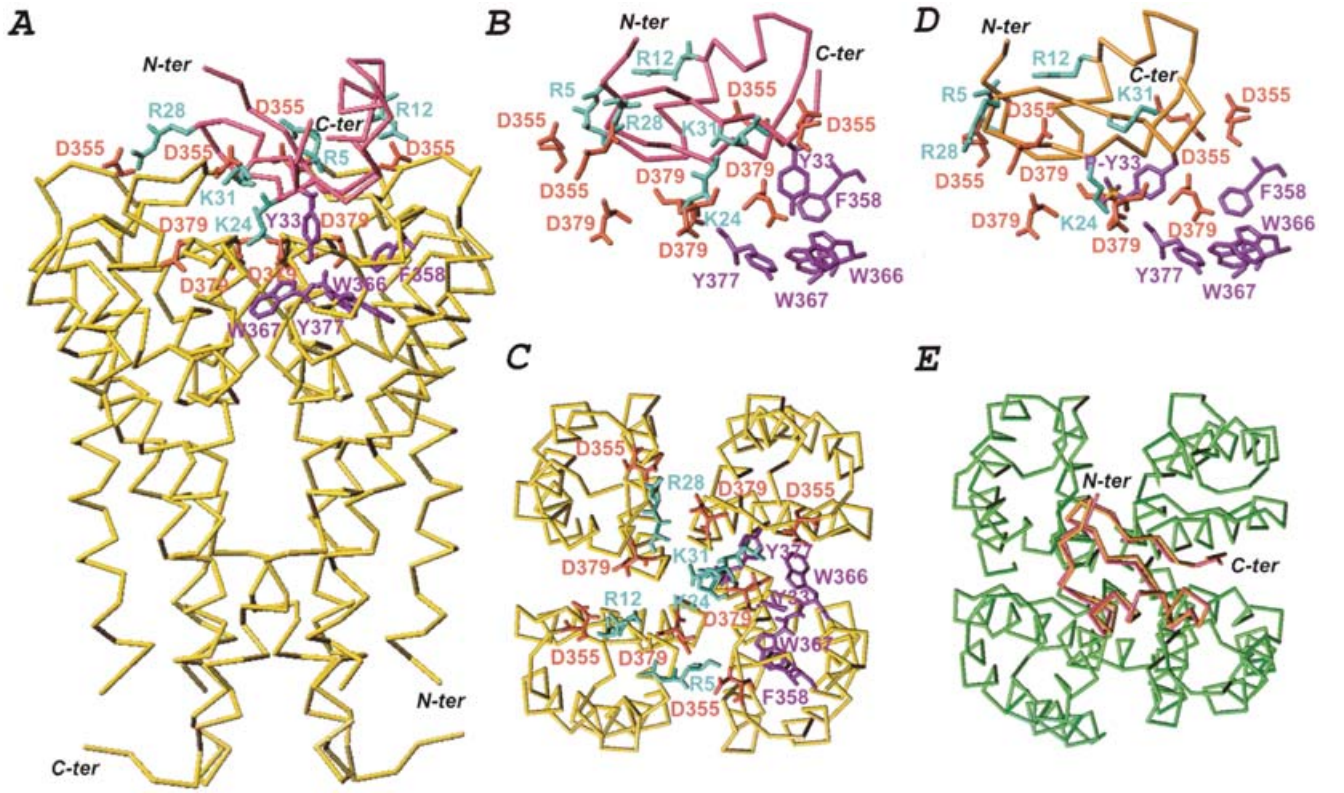


**Figure 6 Docking simulations of Pi1 and P-Pi1 on to rat voltage-gated Kv1.2 channels (pore regions)**

(**A**) Side view (Turbo-Frodo software) depicting the interaction of a molecular model of Pi1 [1–3] with that of the rat voltage-gated Kv1.2 channels (pore regions) [20]. For clarity, C$\alpha$ peptide backbones of only two out of the four S5-P-S6 $\alpha$-subunits of the Kv1.2 channels are presented (yellow). The C$\alpha$ peptide backbone of Pi1 is shown in pink. The side chains of amino acid residues being involved in the Pi1-Kv1.2 channel interaction are detailed. Basic, acidic and aromatic residues are shown in blue, red and purple, respectively. The residues are numbered according to their positions within the Pi1 and Kv1.2 $\alpha$-subunit amino acid sequences [1,2,20]. (**B**) Magnified side view describing the interactions of Pi1 with the voltage-gated Kv1.2 channels. For Pi1, only the side chains of residues involved in this interaction are depicted. Also, only interacting residues from the Kv1.2 $\alpha$-subunits are pictured in their exact 3D positions, according to the ion-channel molecular model (see Figure 1E for details). (**C**) Top view showing the docking [31] of Pi1 on to rat voltage-gated Kv1.2 channels (pore regions). The C$\alpha$ peptide backbone of Pi1 is omitted for clarity. Only interacting residues are presented with their corresponding side chains. The C$\alpha$ peptide backbones of the four S5-P-S6 $\alpha$-subunits of the Kv1.2 channels are shown in yellow. (**D**) Magnified side view describing the interactions of P-Pi1 with the rat voltage-gated Kv1.2 channels. The C$\alpha$ peptide backbone of P-Pi1 is shown in gold. (**E**) Top view corresponding to the superimposed dockings of Pi1 and P-Pi1 C$\alpha$ traces on to rat voltage-gated Kv1.2 channels (pore regions). The C$\alpha$ peptide backbones of Pi1 and P-Pi1 are shown in pink and gold, respectively.

forming a basic ring, might also behave as premium residues with regard to the interaction with this ion channel.

### [$A_{24}$,$A_{33}$]-Pi–Kv1.2 complex

The interaction between [$A_{24}$,$A_{33}$]-Pi1 and the Kv1.2 channel is found to be atypical as compared with Pi1 and P-Pi1 docking solutions (Figure 7). Indeed, the lack of Lys-24 and Tyr-33 of the Pi1 dyad results in Lys-31 side chain entering into the ion channel pore, thereby mimicking the structural role of the Lys-24 side chain. The Pi1 Lys-31 side chain is also surrounded by the four Asp-379 carbonyl oxygen atoms of the P-domain. However, there is clearly no equivalent hydrophobic residue that would functionally replace Tyr-33 contacts. Salt-bridge formation with the basic residues from the basic ring of [$A_{24}$,$A_{33}$]-Pi1 (Arg-5, Arg-12, Arg-28 and Lys-31) is unrelated to that of either Pi1 or P-Pi1. The Arg-5 and Arg-12 residues no longer interact with Asp-355 residues from two adjacent Kv1.2 $\alpha$-subunits. The Arg-28 residue now interacts with Asp-363 (instead of Asp-355), whereas the Lys-31 side chain enters the ionic pore. An additional salt bridge is formed between Lys-3 of [$A_{24}$,$A_{33}$]-Pi1 and Asp-355 of Kv1.2. According to the docking simulation, it appears that the whole positioning of [$A_{24}$,$A_{33}$]-Pi1 over the Kv1.2 channel is clearly distinct from what is observed for Pi1 and P-Pi1. The lack of a 'functional' basic ring in [$A_{24}$,$A_{33}$]-Pi1 may reasonably explain the marked decrease in affinity of this analogue towards Kv1.2 channel, as compared with the affinity of P-Pi1.

### Potential role of a basic ring in toxin binding on to Kv1.2 channels

Conceivably, the contribution of toxin residues other than those belonging to the functional dyad would not be too unexpected, since it is unlikely that only two residues (Lys and either Tyr or Phe), additionally highly conserved among $K^+$ channel-acting toxins, could underlie such marked differences in $K^+$ channel selectivities. To illustrate the potential importance of a basic ring in the recognition and interaction of a toxin with the Kv1.2 channels, we examined the case of scorpion toxin Pi2 (toxin 2 from *P. imperator*) [2,45], whose 3D structure in solution is known [46] (Table 1A, Figure 2D) and which shows activity at picomolar concentrations on to voltage-gated Kv1.2 channels. This toxin possesses a well-defined $\beta$-sheet-associated functional dyad, i.e. Lys-24 and Phe-33. Of note, the usual aromatic Tyr is replaced by an aromatic Phe, which is also thought to interact, via its phenyl ring, with the aromatic cluster (i.e. Phe-358, Trp-366, Trp-367 and Tyr-377) of the Kv1.2 $\alpha$-subunit as well. As shown in Figure 8(A), Pi2 also exhibits a four-member basic ring similar to that of Pi1 or P-Pi1, strengthening the idea of a probable key role of such a ring in the toxin binding on to Kv1.2 channels.

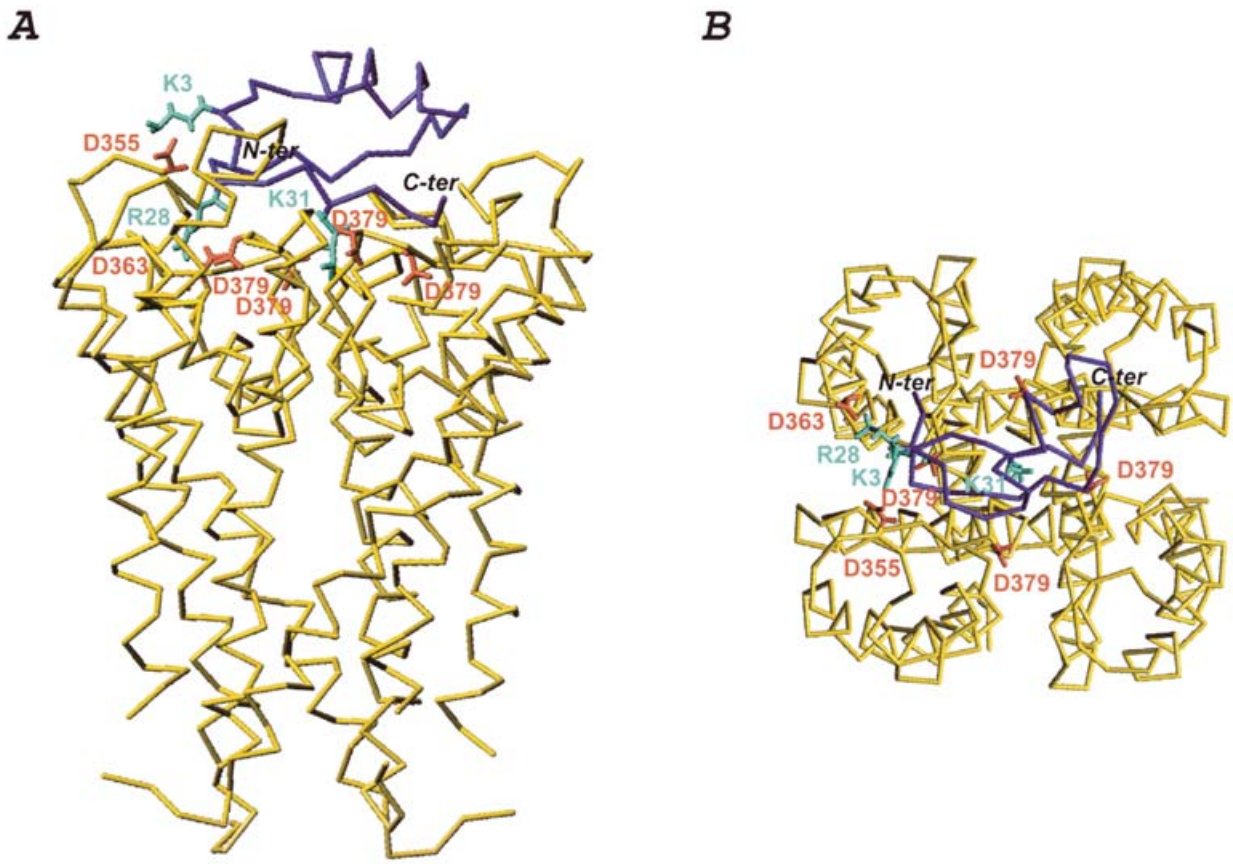


**Figure 7 Docking simulations of [$A_{24}$,$A_{33}$]-Pi1 on to rat voltage-gated Kv1.2 channels**

(**A**) Side view (Turbo-Frodo software) depicting the interaction of a molecular model of [$A_{24}$,$A_{33}$]-Pi1 with that of the voltage-gated Kv1.2 channels. For clarity, C$\alpha$ peptide backbones of only two out of the four S5-P-S6 $\alpha$-subunits of the Kv1.2 channels are presented (yellow). The C$\alpha$ peptide backbone of [$A_{24}$,$A_{33}$]-Pi1 is shown in blue. The side chains of amino acid residues being involved in the [$A_{24}$,$A_{33}$]-Pi1-Kv1.2 channel interaction are detailed. Basic and acidic residues are shown in blue and red, respectively. (**B**) Top view showing the docking of [$A_{24}$,$A_{33}$]-Pi1 on to rat voltage-gated Kv1.2 channels. Only interacting residues are presented with their corresponding side chains. The C$\alpha$ peptide backbones of the four S5-P-S6 $\alpha$-subunits of the Kv1.2 channels are shown in yellow.

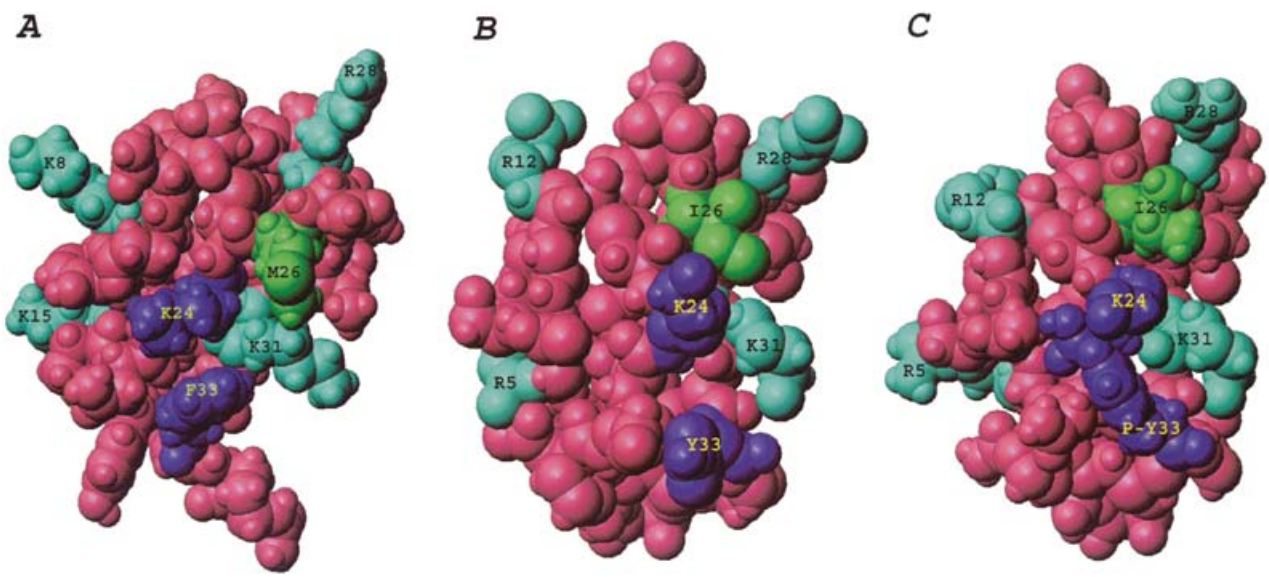


**Figure 8 Functional maps of Pi2, Pi1 and P-Pi1 towards voltage-gated Kv1.2 channels**

(**A**–**C**) Functional maps of Pi2 [2,45,46], Pi1 [1–3] and P-Pi1, respectively. The molecular models (Pi1, P-Pi1) and 3D structure of Pi2 [46] is shown according to a space-filling representation (Turbo-Frodo software). The highlighted amino acid residues are those belonging to the toxin functional maps with regard to the Kv1.2 channels. These residues are numbered according to the peptide amino acid sequences. The basic and hydrophobic residues of the toxin functional maps are pictured in blue and green, respectively. Residues from the functional dyad, as well as the phosphate moiety of Tyr-33 (P-Pi1) are shown in purple. Other residues are shown in pink.

To support experimentally the potential importance of the Pi1 basic ring in toxin interaction with Kv1.2, a first set of three Pi1 analogues were synthesized, in which one or two basic residues from the ring were replaced by Ala, i.e. [$A_{31}$]-Pi1, [$A_5$,$A_{12}$]-Pi1 and [$A_5$,$A_{31}$]-Pi1. These peptides were tested for their effects on Kv1.2 $K^+$ currents. The $IC_{50}$ values obtained were $383 \pm 33$ nM ([$A_{31}$]-Pi1, $n = 5$), $67 \pm 6$ nM ([$A_5$,$A_{12}$]-Pi1, $n = 4$) and $623 \pm 68$ nM ([$A_5$,$A_{31}$]-Pi1, $n = 4$), which should be compared with an $IC_{50}$ value of $1.3 \pm 0.1$ nM for Pi1. Therefore, replacements of these basic residues from the basic ring produced a 51–480-fold reduction in the peptide affinity for Kv1.2 channel. These data strengthen the hypothesis that the basic ring contributes to toxin interaction with Kv1.2. Because the replacement of one or two basic residues from the basic ring did not abolish Pi1 activity, it is likely that the simultaneous presence of all four basic residues is not mandatory for peptide binding on to Kv1.2 channels. A stabilization of the complex could presumably also occur with a reduced number of salt bridges. From the docking experiments, Asp-355 of each Kv1.2 $\alpha$-subunit is pivotal (via salt bridge formation) regarding the interaction of Pi1 or P-Pi1 with this channel. It is interesting to note that such an Asp-355 residue is not present in the $\alpha$-subunits of rat Kv1.1 (Glu-353 instead; see Figure 1D and Table 1B) and rat Kv1.3 (replaced by Ser-375; see Figure 1F and Table 1B) channel subtypes [20], for which Pi-1 and P-Pi1 were found to have no affinity. Based on the molecular model of the rat Kv1.1 channel (Figures 1A–1D), Glu-353 residues of the Kv1.1 $\alpha$-subunits are not expected to form salt bridges with the side chains of Arg-5, Arg-12, Arg-28 and Lys-31 residues of Pi1 or P-Pi1, since they are found to be already connected, by salt bridges, with adjacent His-355 residues (Kv1.1 $\alpha$-subunits; see Figure 1D). In the case of the rat Kv1.3 channel, the nature of Ser-375 (Kv1.3 $\alpha$-subunit; see Figure 1F) does not allow any salt-bridge formation that would stabilize a potential binding of the toxin.

### Functional maps of Pi1 and P-Pi1 towards rat Kv1.2 channels

Results from the docking experiments (Figure 6) [31] allow us to propose deduced functional maps for Pi1 and P-Pi1 (Figures 8B and 8C). These maps suggest an important contribution of Arg-5, Arg-12, Lys-24 (dyad), Ile-26, Arg-28, Lys-31 and Tyr-33 (dyad) residues of Pi1 and P-Pi1 to their recognition and blockage of rat Kv1.2 channels. We therefore suggest a two-level toxin-binding pictorial view in which the toxin basic ring composed of Arg-5, Arg-12, Arg-28 and Lys-31 first acts (via electrostatic forces) in the recognition, interaction and correct positioning of Pi1 and P-Pi1 on to the Kv1.2 channels, and then a tighter interaction takes place through both hydrophobic forces and hydrogen bonding between Tyr-33 (dyad) and the aromatic cluster consisting of Phe-358, Trp-366, Trp-367 and Tyr-377, and between Ile-26 and Val-381. The Lys-24 (dyad) side chain enters the ion-channel pore and is stabilized by the four Asp-379 carbonyl oxygen atoms of the Kv1.2 $\alpha$-subunits; the Lys side chain presumably acts by blocking $K^+$ ion efflux, and might be thereby involved in the toxin-blocking efficacy.

## Concluding remarks

A number of previous structure–activity relationship studies on different scorpion toxins that act on voltage-gated $K^+$ channels suggested that the $\beta$-sheet structure plays a key role in toxin action towards these channels [13,15]. Among the amino acid residues belonging to the $\beta$-sheet, most work has focused on a pair of well-defined basic and aromatic residues, referred to as the functional dyad [13,15–17]. Here, we have examined the relative contribution of the Pi1 functional dyad (i.e. Lys-24 and Tyr-33) to the toxin action on the voltage-gated Kv1.2 channel [1–3,20]. By selective addition of a phosphate moiety on to the Tyr-33 phenol ring, we altered the toxin dyad and the resulting peptide, P-Pi1, remains capable of blocking Kv1.2 channel currents (albeit at a reduced level when compared with Pi1). This indicates that the complete integrity of the Pi1 dyad is not a full prerequisite to the toxin action on Kv1.2 channels, suggesting that the dyad is not the sole determinant in the interaction with this ion channel. This was further confirmed, but to a lesser extent, by the specific activity of [$A_{24}$,$A_{33}$]-Pi1 lacking the dyad on the Kv1.2 channels. The docking simulations [31] of Pi1 and P-Pi1 on to the Kv1.2 channels clearly provide new insights into the structural basis of this recognition/interaction. On the side of the toxin, an unexpected contribution of a basic ring composed of four residues belonging to various domains of the molecule has been highlighted, which further supports the idea of a multipoint interaction between Pi1 and this ion channel. It is noteworthy that such a basic ring is also observed in other potent Kv1.2 channel-acting scorpion toxins (e.g. Pi2 [2,45,46]). At the level of the Kv1.2 channel, a key functional residue appears to be Asp-355 of the $\alpha$-subunit, suggesting that site-directed mutagenesis experiments should be first targeted at this particular position. The production by chemical peptide synthesis of some other selected Pi1 structural analogues, notably those with an altered basic ring, will further confirm experimentally the Pi1 functional map that is deduced from the docking experiments. Because the latter also gave some structural data that might potentially explain the selectivity of the Pi1 action on voltage-gated Kv1.2 channels, we will use the docking simulation approach to design novel Pi1 analogues that exhibit some changes in pharmacological selectivity or affinity towards the voltage-gated $K^+$ channels. Additionally, the present study will be extended to other Kv-channel-acting scorpion toxins, such as Pi2, to tentatively unravel the precise molecular basis of the toxin to Kv-channel recognition.

The authors wish to thank Dr P. Mansuelle for peptide sequencing and amino acid analysis. Professor H. Rochat, Dr C. Devaux and Dr B. De Rougé are acknowledged for helpful discussions. This work was supported by funds from the CNRS and Cellpep SA (Paris, France). A. M. is a recipient of a fellowship from Cellpep SA.

## REFERENCES

1 Olamendi-Portugal, T., Gomez-Lagunas, F., Gurrola, G. B. and Possani, L. D. (1996) A novel structural class of $K^+$-channel blocking toxin from the scorpion *Pandinus imperator*. Biochem. J. **315**, 977–981

2 Rogowski, R. S., Collins, J. H., O'Neill, T. J., Gustafson, T. A., Werkman, T. R., Rogawski, M. A., Tenenholz, T. C., Weber, D. J. and Blaustein, M. P. (1996) Three new toxins from the scorpion *Pandinus imperator* selectively block certain voltage-gated $K^+$ channels. Mol. Pharmacol. **50**, 1167–1177

3 Fajloun, Z., Carlier, E., Lecomte, C., Geib, S., di Luccio, E., Bichet, D., Mabrouk, K., Rochat, H., De Waard, M. and Sabatier, J. M. (2000) Chemical synthesis and characterization of Pi1, a scorpion toxin from *Pandinus imperator* active on $K^+$ channels. Eur. J. Biochem. **267**, 5149–5155

4 Fajloun, Z., Mosbah, A., Carlier, E., Mansuelle, P., Sandoz, G., Fathallah, M., di Luccio, E., Devaux, C., Rochat, H., Darbon, H. et al. (2000) Maurotoxin *Versus* Pi1/HsTx1 toxins: toward new insights in the understanding of their distinct disulfide bridge patterns. J. Biol. Chem. **275**, 39394–39402

5 Delepierre, M., Prochnicka-Chalufour, A. and Possani, L. D. (1997) A novel potassium channel blocking toxin from the scorpion *Pandinus imperator*: a $^1$H NMR analysis using a nano-NMR probe. Biochemistry **36**, 2649–2658

6 Bontems, F., Roumestand, C., Gilquin, B., Ménez, A. and Toma, F. (1991) Refined structure of charybdotoxin: common motifs in scorpion toxins and insect defensins. Science **254**, 1521–1523

7 Kharrat, R., Mabrouk, K., Crest, M., Darbon, H., Oughideni, R., Martin-Eauclaire, M. F., Jacquet, G., El Ayeb, M., Van Rietschoten, J., Rochat, H. and Sabatier, J. M. (1996) Chemical synthesis and characterization of maurotoxin, a short scorpion toxin with four disulfide bridges that acts on $K^+$ channels. Eur. J. Biochem. **242**, 491–498

8 Kharrat, R., Mansuelle, P., Sampieri, F., Crest, M., Oughideni, R., Van Rietschoten, J., Martin-Eauclaire, M. F., Rochat, H. and El Ayeb, M. (1997) Maurotoxin, a four disulfide bridge toxin from *Scorpio maurus* venom: purification, structure and action on potassium channels. FEBS Lett. **406**, 284–290

9 Lebrun, B., Romi-Lebrun, R., Martin-Eauclaire, M. F., Yasuda, A., Ishiguro, M., Oyama, Y., Pongs, O. and Nakajima, T. (1997) A four-disulphide-bridged toxin, with high affinity towards voltage-gated $K^+$ channels, isolated from *Heterometrus spinnifer* (Scorpionidae) venom. Biochem. J. **328**, 321–327

10 Tytgat, J., Chandy, G., Garcia, M. L., Gutman, G. A., Martin Eauclaire, M. F., van der Walt, J. J. and Possani, L. D. (1999) A unified nomenclature for short-chain peptides isolated from scorpion venoms: alpha-KTx. Trends Physiol. Sci. **20**, 444–447

11 Sabatier, J. M., Zerrouk, H., Darbon, H., Mabrouk, K., Benslimane, A., Rochat, H., Martin-Eauclaire, M. F. and Van Rietschoten, J. (1993) P05, a new leiurotoxin I-like scorpion toxin: synthesis ans structure-activity relationships of the $\alpha$-amidated analog, a ligand of $Ca^{2+}$-activated $K^+$ channels with increased affinity. Biochemistry **32**, 2763–2770

12 Sabatier, J. M., Fremont, V., Mabrouk, K., Crest, M., Darbon, H., Rochat, H., Van Rietschoten, J. and Martin-Eauclaire, M. F. (1994) Leiurotoxin I, a scorpion toxin specific for $Ca^{2+}$-activated $K^+$ channels: structure-activity analysis using synthetic analogs. Int. J. Peptide Protein Res. **43**, 486–495

13 Darbon, H., Blanc, E. and Sabatier, J. M. (1999) Three-dimensional structure of scorpion toxins: towards a new model of interaction with potassium channels. In Perspectives in Drug Discovery and Design: Animal Toxins and Potassium Channels, vol. 15/16 (Darbon, H. and Sabatier, J. M., eds.), pp. 40–60, Kluwer/Escom, Kluwer Academic Publishers, Dordrecht

14 Shakkottai, V. G., Regaya, I., Wulff, H., Fajloun, Z., Tomita, H., Fathallah, M., Cahalan, M. D., Gargus, J. J., Sabatier, J. M. and Chandy, K. G. (2001) Design and characterization of a highly selective peptide inhibitor of the small conductance calcium-activated $K^+$ channel, SKCa2. J. Biol. Chem. **276**, 43145–43151

15 Possani, L. D., Selisko, B. and Gurrola, G. B. (1999) Structure and function of scorpion toxins affecting $K^+$ channels. In Perspectives in Drug Discovery and Design: Animal Toxins and Potassium Channels, vol 15/16 (Darbon, H. and Sabatier, J. M., eds.), pp. 15–40, Kluwer/Escom, Kluwer Academic Publishers, Dordrecht

16 Dauplais, M., Lecoq, A., Song, J., Cotton, J., Jamin, N., Gilquin, B., Roumestand, C., Vita, C., de Meideros, C. L., Rowan, E. G. et al. (1997) On the convergent evolution of animal toxins. Conservation of a diad of functional residues in potassium channel-blocking toxins with unrelated structures. J. Biol. Chem. **272**, 4302–4309

17 Srinivasan, K. N., Sivaraja, V., Huys, I., Sasaki, T., Cheng, B., Kumar, T. K., Sato, K., Tytgat, J., Yu, C., San, B. C. et al. (2002) Hefutoxin1, a novel toxin from the scorpion *Heterometrus fulvipes* with unique structure and function: importance of the functional diad in potassium channel selectivity. J. Biol. Chem. **277**, 30040–30047

18 Merrifield, R. B. (1986) Solid phase synthesis. Science **232**, 341–347

19 Morais Cabral, J. H., Lee, A., Cohen, S. L., Chait, B. T., Li, M. and Mackinnon, R. (1998) The structure of the potassium channel: molecular basis of $K^+$ conduction and selectivity. Science **280**, 69–77

20 Christie, M. J. (1995) Molecular and functional diversity of $K^+$ channels. Clin. Exp. Pharmacol. Physiol. **22**, 944–951

21 Roussel, A. and Cambillau, C. (1989) Silicon Graphics Geometry Partner Directory, pp. 77–78, Silicon Graphics, Mountain View, CA

22 Reference deleted.

23 Brünger, A. T., Adams, P. D., Clore, G. M., DeLano, W. L., Gros, P., Grosse-Kunstleve, R. W., Jiang, J. S., Kuszewski, J., Nilges, M., Pannu, N. S. et al. (1998) Crystallography and NMR system (CNS): a new software system for macromolecular structure determination. Acta Crystallogr. **D54**, 905–921

24 Higgins, D., Thompson, J., Gibson, T., Thompson, J. D., Higgins, D. G. and Gibson, T. J. (1994) CLUSTAL W: improving the sensitivity of progressive multiple sequence alignment through sequence weighting, position-specific gap penalties and weight matrix choice. Nucleic Acids Res. **22**, 4673–4680

25 Altschul, S. F., Madden, T. L., Schäffer, A. A., Zhang, J., Zhang, Z., Miller, W. and Lipman, D. J. (1997) Gapped BLAST and PSI-BLAST: A new generation of protein database search programs. Nucleic Acids Res. **25**, 3389–3402

26 Altschul, S. F. (1991) Amino acid substitutions matrices from an information theoretic perspective. J. Mol. Biol. **219**, 555–665

27 Blanc, E., Sabatier, J. M., Kharrat, R., Meunier, S., El Ayeb, M., Van Rietschoten, J. and Darbon, H. (1997) Solution structure of maurotoxin, a scorpion toxin from *Scorpio maurus*, with high affinity for voltage-gated potassium channels. Proteins **29**, 321–333

28 Hooft, R. W. W., Vriend, G., Sander, C. and Abola, E. E. (1996) Errors in protein structures. Nature (London) **381**, 272

29 Morris, A. L., MacArthur, M. W., Hutchinson, E. G. and Thornton, J. M. (1992) Stereochemical quality of protein structure coordinates. Proteins **12**, 345–364

30 Laskowski, R. A., MacArthur, M. W., Moss, D. S. and Thornton, J. M. (1993) PROCHECK: A program to check the stereochemical quality of protein structures. J. Appl. Crystallogr. **26**, 283–291

31 Palma, P. N., Krippahl, L., Wampler, J. E. and Moura, J. J. G. (2000) BiGGER: a new (soft) docking algorithm for predicting protein interactions. Proteins Struct. Funct. Genet. **39**, 372–384

32 Gilquin, B., Racape, J., Wrisch, A., Visan, V., Lecoq, A., Grissmer, S., Ménez, A. and Gasparini, S. (2002) Structure of the BgK-Kv1.1 complex based on distance restraints identified by double mutant cycles. Molecular basis for convergent evolution of Kv1 channel blockers. J. Biol. Chem. **277**, 37406–37413

33 Alessandri-Haber, N., Lecoq, A., Gasparini, S., Grangier-Macmath, G., Jacquet, G., Harvey, A. L., de Medeiros, C., Rowan, E. G., Gola, M., Ménez, A. and Crest, M. (1999) Mapping the functional anatomy of BgK on Kv1.1, Kv1.2, and Kv1.3. Clues to design analogs with enhanced selectivity. J. Biol. Chem. **274**, 35653–35661

34 Gasparini, S., Danse, J. M., Lecoq, A, Pinkasfeld, S., Zinn-Justin, S., Young, L. C., de Medeiros, C. C., Rowan, E. G., Harvey, A. L. and Ménez, A. (1998) Delineation of the functional site of alpha-dendrotoxin. The functional topographies of dendrotoxins are different but share a conserved core with those of other Kv1 potassium channel-blocking toxins. J. Biol. Chem. **273**, 25393–25403

35 Harvey, A. L., Vatanpour, H., Rowan, E. G., Pinkasfeld, S., Vita, C., Ménez, A. and Martin-Eauclaire, M. F. (1995) Structure-activity studies on scorpion toxins that block potassium channels. Toxicon **33**, 425–436

36 Fu, W., Cui, M., Briggs, J. M., Huang, X., Xiong, B., Zhang, Y., Luo, X., Shen, J., Ji, R., Jiang, H. and Chen, K. (2002) Brownian dynamics simulations of the recognition of the scorpion toxin maurotoxin with the voltage-gated potassium ion channels. Biophys. J. **83**, 2370–2385

37 Cui, M., Shen, J., Briggs, J. M., Fu, W., Wu, J., Zhang, Y., Luo, X., Chi, Z., Ji, R., Jiang, H. and Chen, K. (2002) Brownian dynamics simulations of the recognition of the scorpion toxin P05 with the small-conductance calcium-activated potassium channels. J. Mol. Biol. **318**, 417–428

38 Koch, R. O., Wanner, S. G., Koschak, A., Hanner, M., Schwarzer, C., Kaczorowski, G. J., Slaughter, R. S., Garcia, M. L. and Knaus, H. G. (1997) Complex subunit assembly of neuronal voltage-gated $K^+$ channels. Basis for high-affinity toxin interactions and pharmacology. J. Biol. Chem. **272**, 27577–27581

39 Gray, E. G. and Whittaker, V. P. (1962) The isolation of nerve endings from brain: an electron microscopic study of cell fragments derived by homogenization centrifugation. J. Anat. **96**, 79–88

39a Seagar, M. J., Granier, C. and Couraud, F. (1984) Interactions of the neurotoxin apamin with a $Ca^{2+}$-activated $K^+$ channel in primary neuronal cultures. J. Biol. Chem. **259**, 1491–1495

40 De Waard, M. and Campbell, K. P. (1995) Subunit regulation of the neuronal alpha 1A $Ca^{2+}$ channel expressed in *Xenopus* oocytes. J. Physiol. **485**, 619–634

41 Eppig, J. J. and Dumont, J. N. (1976) Defined nutrient medium for the *in vitro* maintenance of *Xenopus laevis* oocytes. In Vitro **12**, 418–427

42 Grissmer, S., Nguyen, A. N., Aiyar, J., Hanson, D. C., Mather, R. J., Gutman, G. A., Karmilowicz, M. J., Auperin, A. A. and Chandy, K. G. (1994) Pharmacological characterization of five cloned voltage-gated $K^+$ channels, types Kv 1.1, 1.2, 1.3, 1.5, and 3.1, stably expressed in mammalian cell lines. Mol. Pharmacol. **45**, 1227–1234

43 Batista, C. V., Gomez-Lagunas, F., Rodriguez de la Vega, R. C., Hajdu, P., Panyi, G., Gaspar, R. and Possani, L. D. (2002) Two novel toxins from the Amazonian scorpion *Tityus cambridgei* that block Kv1.3 and *Shaker* B $K^+$ channels with distinctly different affinities. Biochem. Biophys. Acta **1601**, 123–131

44 Castle, N. A., London, D. O., Creech, C., Fajloun, Z., Stocker, J. W. and Sabatier, J. M. (2003) Maurotoxin: a potent inhibitor of intermediate conductance $Ca^{2+}$-activated potassium channels. Mol. Pharmacol. **63**, 1–10

45 Gomez-Lagunas, F., Olamendi-Portugal, T., Zamudio, F. Z. and Possani, L. D. (1996) Two novel toxins from the venom of the scorpion *Pandinus imperator* show that the N-terminal amino acid sequence is important for their affinities towards *Shaker* B $K^+$ channels. J. Membr. Biol. **152**, 49–56

46 Tenenholz, T. C., Rogowski, R. S., Collins, J. H., Blaustein, M. P. and Weber, D. J. (1997) Solution structure for *Pandinus* toxin K-alpha (PiTX-K alpha), a selective blocker of A-type potassium channels. Biochemistry **36**, 2763–2771


Received 14 January 2003/8 September 2003; accepted 9 September 2003
Published as BJ Immediate Publication 9 September 2003, DOI 10.1042/BJ20030115